Modeling Airspace Stability and Capacity for Decentralized Separation

Sunil, Emmanuel; Ellerbroek, Joost; Hoekstra, Jacco; Maas, Jerom

Publication date
2017

Document Version
Final published version

Published in
12th Seminar Papers

Twelfth USA/Europe Air Traffic Management Research and Development Seminar (ATM2017)

Modeling Airspace Stability and Capacity for Decentralized Separation

Emmanuel Sunil, Joost Ellerbroek, Jacco Hoekstra and Jerom Maas
Control and Simulation, Faculty of Aerospace Engineering
Delft University of Technology (TU Delft)
Delft, The Netherlands

***Abstract*—In the context of decentralized separation, airspace stability pertains to the propagation of conflict chain reactions as a result of tactical conflict resolution maneuvers. This notion of airspace stability has been used in previous literature to develop a semi-empirical method for determining the capacity of a decentralized direct-routing airspace concept in the horizontal plane. The present paper extends this method by explicitly modeling: a) the effect of a given Conflict Detection and Resolution (CD&R) strategy on the stability of the airspace; b) the influence of direct-routing on instantaneous conflict probability; and c) the impact of finite-time measurements on the determination of airspace states. To validate the resulting analytical capacity model, fast-time simulations were performed. The results indicate that the predictions of the analytical model are close to that of the previous semi-empirical approach. Thus, the analytical model can be used to obtain a first-order estimate of the maximum theoretical capacity, as along as simulation settings do not cause the 'local', or per aircraft, conflict rate to deviate significantly from assumptions made during the model derivation. Future work will focus on relaxing model assumptions, and extending the modeling approach to three-dimensional airspace.**

***Keywords*—ATM performance measurement; airspace capacity models; airspace stability; Domino Effect Parameter (DEP); decentralized separation; self-separation; BlueSky ATM simulator**

NOMENCLATURE

C	=	Conflict Count
N	=	Aircraft Count
p_2	=	Instantaneous conflict probability between two aircraft
p_s	=	Effect of structure on on instantaneous conflict probability
V	=	True Airspeed
t_l	=	Conflict Detection look-ahead time
D_{sep}	=	Horizontal separation minimum
A	=	Airspace area
T	=	Analysis time
$\bar{L}$	=	Average flight distance
k_{cdr}	=	Extra distance searched for conflicts due to CD&R
r_c	=	Rate of conflict per aircraft per unit distance
ρ	=	Traffic density
Subscripts:		
$_{wr}$	=	With conflict resolution
$_{nr}$	=	Without conflict resolution
$_{ss}$	=	Steady State/Instantaneous
$_{total}$	=	Total
$_{max}$	=	Maximum

I. INTRODUCTION

Decentralization of traffic separation responsibility, from ground based Air Traffic Controllers (ATCo) to each individual aircraft, has been proposed as a means to improve airspace capacity [1]–[3]. To support decentralization, significant research effort has been devoted towards the design of novel Conflict Detection and Resolution (CD&R) algorithms [4]. However, the extent to which decentralization affects airspace capacity is not well understood. Moreover, conventional capacity modeling methods, such as those related to ATCo workload, are not relevant for decentralized control.

To develop appropriate capacity modeling methods, it is first necessary to establish a commonly accepted definition of capacity for decentralization. At a fundamental level, capacity, regardless of location or type of separation management, can be considered equivalent to the density at which the airspace becomes saturated, i.e., the density beyond which no further demand can be accommodated without significantly degrading macroscopic system properties such as safety and efficiency.

In line with this view of capacity, previous research has identified airspace stability, which considers the propagation of conflicts as a result of tactical conflict resolution maneuvers, as an important metric to determine the saturation density of decentralized airspace [5], [6]. These studies have shown that tactical conflict resolutions can destabilize the airspace at high traffic densities by triggering conflict chain reactions due to the scarcity of airspace and due to the type of CD&R algorithm used. Previous work has also presented the Domino Effect Parameter (DEP) as a measure of stability [5], [6], and it has been used to develop a semi-empirical model to determine the capacity of a decentralized direct-routing airspace concept in horizontal plane [7]. While this approach provides an innovative and practical means of measuring capacity for decentralization, it requires time consuming simulations to asses the factors affecting capacity for different airspace configurations and/or CD&R strategies.

This paper extends the aforementioned *semi-empirical* approach by explicitly modeling the effect of a given CD&R algorithm on airspace stability, and by taking into account the influence of direct-routing on instantaneous conflict probability (the later from our prior work). Additionally, the impact of finite-time measurements on the determination of airspace states has also been considered to further improve the accuracy of the resulting *analytical* capacity model. This model is parametrized by physical airspace and CD&R parameters, and it is intended to obtain a first-order estimate of airspace capacity, and to study the factors affecting capacity.

To validate the derived model, fast-time simulations of a decentralized direct-routing airspace concept in the horizontal plane are performed. Simulations are performed for several traffic demand densities, and for multiple values of model relevant CD&R parameters. Here 'state-based' conflict detection and the Modified Voltage Potential (MVP) conflict resolution algorithms are used as a case-study. The accuracy of the modeling approach is evaluated by comparing model predictions to those determined using the semi-empirical method.

This paper begins with an overview of the most relevant aspects of prior work in section II. In section III, an analytical model of airspace stability and capacity is derived. This is followed in sections IV and V with the design and results of fast-time simulations used to validate the analytical model. Finally, the main conclusions are summarized in section VI.

II. PREVIOUS RESEARCH

The analytical capacity model developed in this paper builds on previous research on measuring airspace stability and

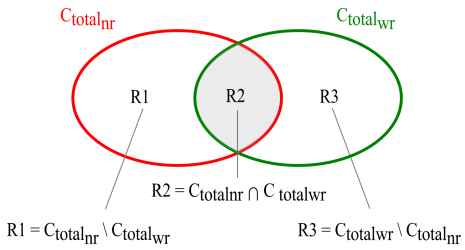

Fig. 1. The Domino Effect Parameter (DEP) compares simulations with and without Conflict Resolution (CR) to measure airspace stability

capacity, and on modeling instantaneous conflict probability. This section provides an overview of these topics.

A. Measuring Airspace Stability

Airspace stability relates to the occurrence and propagation of conflict chain reactions when tactical Conflict Resolution (CR) is used. Stability can be measured using the Domino Effect Parameter (DEP) [5], [6], and can be visualized using the Venn diagram in Fig. 1. Here, $C_{total_{nr}}$ is the set of all conflicts without CR, and $C_{total_{wr}}$ is the set of all conflicts with CR, for identical traffic scenarios. Furthermore, three regions can be identified in Fig. 1; $R1$, $R2$ and $R3$. By comparing $R3$ with $R1$, the proportion of 'destabilizing' conflicts caused by CR can be determined. Thus, the DEP is defined as [5], [6]:

$$DEP = \frac{R3 - R1}{C_{total_{nr}}} = \frac{C_{total_{wr}}}{C_{total_{nr}}} - 1 \tag{1}$$

A high DEP value implies high airspace instability. Note that *conflicts are defined as predicted losses of separation*.

B. Relating Airspace Stability to Capacity

Using the DEP, a semi-empirical model to measure the capacity of a decentralized direct-routing airspace concept in the horizontal plane was developed in [7]. In that paper, expressions for $C_{total_{nr}}$ and $C_{total_{wr}}$ were formulated in terms of airspace parameters, and were substituted into Eq. 1 to approximate the DEP as:

$$DEP \approx \frac{\rho_{ac}}{\rho_{max} - \rho_{ac}} \tag{2}$$

Here, ρ_{ac} is traffic density, and the term ρ_{max} is defined to be the maximum theoretical capacity of the airspace because the DEP, and therefore the number of conflict chain reactions, becomes infinite when ρ_{ac} approaches ρ_{max}. In [7] ρ_{max} was expressed as:

$$\rho_{max} = \frac{1}{D_{sep} \cdot k_{cdr} \cdot p_s} \tag{3}$$

Where D_{sep} is the horizontal separation minimum, k_{cdr} accounts for the effect of CD&R on airspace stability, and p_s is the effect of traffic/route structure on the instantaneous conflict probability without CR. Since no explicit analytical models for k_{cdr} and p_s were discussed in [7], a semi-empirical approach was proposed to determine capacity, i.e., by determining the ρ_{max} that fit the DEP logged during fast-time simulations to Eq. 2 in a least-square sense.

C. Relating Traffic Structure to Instantaneous Conflict Probability Without Conflict Resolution

Our prior work on different methods of structuring traffic revealed that relative velocity played an important role on the instantaneous conflict probability between two aircraft [8]. This understanding was subsequently used to model the relationship between these two variables for motion in the horizontal plane without CR [9]:

$$p_s = \frac{2\pi}{\alpha}\left(1 - \frac{2}{\alpha}\sin\frac{\alpha}{2}\right) \tag{4}$$

Here, α is the magnitude of the allowed heading range for aircraft cruising at the same flight level (e.g. 180^o for the hemispheric rule). This expression is valid for the case where all aircraft have equal airspeed. For airspace with no constraints, i.e., direct-routing airspace, $\alpha = 360^o = 2\pi$ rad, and thus $p_s = 1$.

Since a model for p_s has been developed, the only remaining term that needs to be modeled to extend the semi-empirical method from [7] to an analytical model is k_{cdr}. This is the main contribution of the current paper.

III. Derivation of an Analytical Airspace Stability and Capacity Model

In this section, the semi-empirical method of [7] is extended to an analytical capacity model for 'state-based' Conflict Detection (CD) and the Modified Voltage Potential (MVP) Conflict Resolution (CR) algorithms. The goal of the derivation is to model the DEP in terms of airspace and CD&R parameters. Thus, models for the number of conflicts with and without CR, and a model of the explicit effect of CD&R on stability, are developed.

A. Modeling the Rate and Number of Conflicts Without Conflict Resolution

1) Global Instantaneous Conflict Rate

The modeling process begins with the global instantaneous, or steady-state, conflict rate per unit time for all aircraft without CR, $C_{ss_{nr}}$. As aircraft move independently of each other without CR, $C_{ss_{nr}}$ has been modeled in literature as the expected value of a binomial random variable model that is summed over all aircraft in the airspace [2], [7]:

$$C_{ss_{nr}} = \frac{1}{2}\sum_{i=1}^{N_{ss}}(N_{ss} - 1)\,p_2 = \frac{N_{ss}\,(N_{ss} - 1)}{2}p_2 \tag{5}$$

Here, N_{ss} is the steady-state number of aircraft, and p_2 is the instantaneous conflict probability between any two aircraft. Note that the number of conflicts is divided by 2 in the above expression so that conflicts between the same two aircraft are not counted twice at a given moment in time.

For a conflict to occur between two aircraft, their trajectories must intersect, and the intersection should occur within the look-ahead time, t_l, used for CD. Therefore, p_2 can be computed by multiplying the probabilities for these two events occurring.

The chance that any two trajectories intersect at some point in time, p_s, depends on the route structure, and it has been modeled in our prior work, see Eq. 4. The chance that this intersection occurs within t_l depends on the CD method, and the total airspace area under consideration, A. For 'state-based' CD, aircraft detect conflicts within a 'conflict search area', A_c, defined by t_l, the separation minimum D_{sep} and the average aircraft velocity with no resolution $\bar{V}_{nr}$, see Fig. 2. Conflicts are detected if the Closest Point of Approach (CPA) of an intruder aircraft is located in A_c. Thus p_2 is defined as:

$$p_2 = \frac{A_c}{A}p_s = \frac{2\;D_{sep} \cdot \bar{V}_{nr} \cdot t_l}{A}p_s \tag{6}$$

As mentioned in section II-C, for direct-routing airspace $p_s = 1$. Nonetheless, it is left in the subsequent steps for completeness. Substituting Eq. 6 in Eq. 5 yields the following for $C_{ss_{nr}}$:

$$C_{ss_{nr}} = \frac{N_{ss}\,(N_{ss} - 1)\,(D_{sep} \cdot \bar{V}_{nr} \cdot t_l)}{A}p_s \tag{7}$$

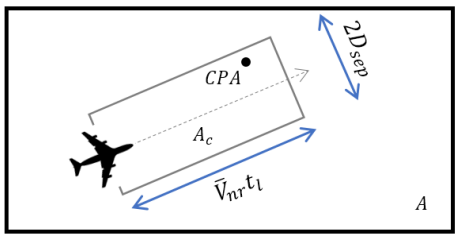

Fig. 2. Area searched for conflicts, A_c, for 'state-based' conflict detection. Here A is the total airspace area under consideration. A conflict occurs if the Closest Point of Approach (CPA) of an intruder aircraft is inside A_c.

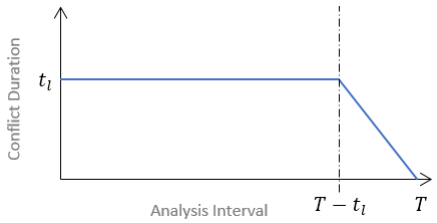

Fig. 3. Conflict duration decreases linearly near the end of a finite analysis time interval T, if conflicts are counted at the time of detection. Here t_l is the CD look-ahead time.

2) Total Number of Conflicts for a Given Time Interval

The total number of conflicts without CR, $C_{total_{nr}}$, can be computed by integrating the global instantaneous conflict rate, $C_{ss_{nr}}$, over an analysis time interval, T, and dividing the result by the average duration of a conflict without CR, $\bar{t}_{c_{nr}}$:

$$C_{total_{nr}} = \frac{1}{\bar{t}_{c_{nr}}} \int_0^T C_{ss_{nr}} = \frac{C_{ss_{nr}}\ T}{\bar{t}_{c_{nr}}} \tag{8}$$

If conflicts are counted at the time of detection, then $\bar{t}_{c_{nr}}$ is equivalent to t_l for infinite time horizons. However, for finite time measurements, as during fast-time simulations, the logged duration, or lifetime, of a conflict decreases linearly at the end of the measurement time interval of length T, see Fig. 3, as logging stops sharply at a specified time. For such cases, $\bar{t}_{c_{nr}}$ can be calculated as the area of the shape under the graph in Fig. 3, over the measurement time interval T:

$$\bar{t}_{c_{nr}} = \frac{Tt_l - \frac{1}{2}t_l^2}{T} = t_l\left(1 - \frac{t_l}{2T}\right) \tag{9}$$

Note that the effect of finite time measurements on conflict counts were not considered in [7]. Using the fact that $N_{ss} = \rho_{ac}\ A$, where ρ_{ac} is airspace density, $C_{total_{nr}}$ can be rewritten by substituting Eq. 9 into Eq. 8:

$$C_{total_{nr}} = \frac{2\ p_s \cdot D_{sep} \cdot \bar{V}_{nr} \cdot T^2 \cdot \rho_{ac} \cdot A\,(\rho_{ac} - 1/A)}{2T - t_l} \tag{10}$$

3) Local Conflict Rate

In addition to the global instantaneous conflict rate, for decentralized traffic it is also necessary to consider the local, or per aircraft, conflict rate per unit *distance* without CR, $r_{c_{nr}}$. To this end, $r_{c_{nr}}$ can be expressed as the ratio between the the total number of conflicts during a single flight without CR, $C_{1_{nr}}$, and the average flight distance of an aircraft through area A without CR, $\bar{L}_{nr}$:

$$r_{c_{nr}} = \frac{C_{1_{nr}}}{\bar{L}_{nr}} \tag{11}$$

Subsequently, $C_{1_{nr}}$ can be written as a function of $C_{total_{nr}}$:

$$C_{1_{nr}} = \frac{C_{total_{nr}}}{N_{total_{nr}}} \tag{12}$$

Here, $N_{total_{nr}}$ is the total number of aircraft that flew through area A during the analysis time interval T without CR. $N_{total_{nr}}$ can be written in terms of known parameters by noting that the rate of introduction of aircraft needed to maintain a constant traffinc density in area A must be equal to $N_{ss} \cdot \bar{V}_{nr}/\bar{L}_{nr}$. Since $N_{ss} = \rho_{ac}\ A$, $N_{total_{nr}}$ can be formulated as:

$$N_{total_{nr}} = \frac{N_{ss}\ \bar{V}_{nr}}{\bar{L}_{nr}}\ T + N_{ss} = \rho_{ac}\ A\left(\frac{\bar{V}_{nr}}{\bar{L}_{nr}}\ T + 1\right) \tag{13}$$

The first term on the right hand side of Eq. 13 is the number of aircraft that started their flights during the analysis time interval, and the second term is the number of aircraft which are already present in the airspace at the start of the analysis time. This second term was not explicitly mentioned in [7], but needs to considered since these aircraft also affect $C_{total_{nr}}$. Using the model of $C_{total_{nr}}$ from Eq. 10, and by substituting Eqs. 12 and 13 into Eq. 11, $r_{c_{nr}}$ can be formulated as:

$$r_{c_{nr}} = \frac{2\ p_s \cdot D_{sep} \cdot \bar{V}_{nr} \cdot T^2\left(\rho_{ac} - \frac{1}{A}\right)}{(2T - t_l)\left(\bar{V}_{nr}\ T + \bar{L}_{nr}\right)} \tag{14}$$

B. Modeling the Rate and Number of Conflicts With Conflict Resolution

When an aircraft performs a CR maneuver, it deviates from its nominal path, see Fig. 4. This increases the total distance flown compared to the case without CR, i.e., green rectangle in Fig. 4. Additionally, for each detected conflict, an extra area of airspace is searched for conflicts, but not flown through, i.e. red rectangle in Fig. 4. Thus when computing the total number of conflicts per unit distance for a single flight, $C_{1_{wr}}$, both these processes need to be taken into account:

$$C_{1_{wr}} = \left(\bar{L}_{nr} + k_{cdr}\ C_{1_{wr}}\right) r_{c_{wr}} \tag{15}$$

Here, $r_{c_{wr}}$ is the rate of conflicts per unit distance for a single aircraft with CR, and the term in the parenthesis is the total distance searched for conflicts during one complete flight. This distance increases linearly with the number of conflicts detected, and the rate of increase of the 'extra' distance searched per conflict, k_{cdr}, is dependent on the selected CD and CR strategy and settings. This parameter is modeled in section III-C. Solving Eq. 15 for $C_{1_{wr}}$ gives:

$$C_{1_{wr}} = \frac{\bar{L}_{nr} \cdot r_{c_{wr}}}{1 - k_{cdr} \cdot r_{c_{wr}}} \tag{16}$$

From $C_{1_{wr}}$, the total number of conflicts during the analysis interval, $C_{total_{wr}}$, can be formulated as:

$$C_{total_{wr}} = C_{1_{wr}}\ N_{total_{wr}} \tag{17}$$

Here, $N_{total_{wr}}$ is the total number of aircraft that flew though area A during the analysis interval T with CR. Substituting Eq. 16 into Eq. 17 results in:

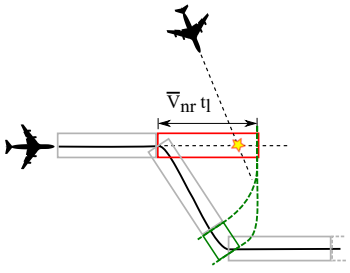

Fig. 4. Resolving conflicts increases the total area of airspace searched for conflicts due to conflict detection (red) and conflict resolution (green). Here, an arbitrary resolution stragety is pictured.

$$C_{total_{wr}} = \frac{N_{total_{wr}} \cdot \bar{L}_{nr} \cdot r_{c_{wr}}}{1 - k_{cdr} \cdot r_{c_{wr}}} \tag{18}$$

To continue the derivation of $C_{total_{wr}}$, [7] uses two assumptions to relate the cases with and without CR:

1) $N_{total_{wr}} \approx N_{total_{nr}}$: Although CR increases traffic density due to longer flights, it is also expected to increase the average distance flown by proportional amount. Thus the total number of aircraft is not to expected vary significantly with CR, as can be seen by applying this rationale to Eq. 13.
2) $r_{c_{wr}} \approx r_{c_{nr}}$: This assumption stems from the fact that there are no preferred directions/routes for a decentralized direct-routing airspace concept. Hence conflicts are equally likely in all directions, and performing conflict resolutions is *not* expected to change the rate of conflicts per unit distance for a single flight compared to the case without CR. This also implies that the total number of conflicts for a single flight is higher with CR, as resolutions increase the total amount of airspace searched for conflicts, as illustrated by Eq. 15.

These assumptions are also used in this work, and their validity will be examined in section V. Using these assumptions, the expression for $C_{total_{wr}}$ can be rewritten to use $N_{total_{nr}}$ (Eq. 13) and $r_{c_{nr}}$ (Eq. 14):

$$\begin{aligned} C_{total_{wr}} &\approx \frac{N_{total_{nr}} \cdot \bar{L}_{nr} \cdot r_{c_{nr}}}{1 - k_{cdr} \cdot r_{c_{nr}}} \\ &\approx \frac{\rho_{ac}\ A\ \Upsilon\ (\bar{V}_{nr}\ T + \bar{L}_{nr})}{(2T - t_l)\ (\bar{V}_{nr}\ T + \bar{L}_{nr}) - k_{cdr}\ \Upsilon} \end{aligned} \tag{19}$$

Here, Υ is defined as:

$$\Upsilon = 2\ p_s \cdot D_{sep} \cdot \bar{V}_{nr} \cdot T^2 \left(\rho_{ac} - \frac{1}{A}\right) \tag{20}$$

C. Modeling the Extra Distance Searched Per Conflict Resolution Maneuver

As mentioned earlier, $C_{total_{wr}}$ is dependent on k_{cdr}, which is the extra distance searched for conflicts, per conflict resolution maneuver. From Fig. 4, it can be seen that k_{cdr} is composed of two components; 1) the extra distance searched due to CD, k_{cd}, and 2) the extra distance searched due CR, k_{cr}. Therefore, k_{cdr} can be expressed as:

$$k_{cdr} = k_{cd} + \bar{k}_{cr} \tag{21}$$

A large value of k_{cdr} increases the amount of extra airspace searched for conflicts, and thus also increases the chance of conflict chain reactions. Therefore k_{cdr} is strongly related to airspace stability, and is dependent on the underlying algorithms and settings used for CD and CR. Below, models for k_{cd} and k_{cr} are developed for 'state-based' CD and for the Modified Voltage Potential (MVP) CR algorithm.

1) Extra Distance Searched Due to Conflict Detection

For every detected conflict, an extra area of airspace is searched for conflicts, but not flown through. For 'state-based' CD, this distance, k_{cd}, corresponds to the length of the red rectangle in Fig. 4:

$$k_{cd} = \bar{V}_{nr}\ t_l \tag{22}$$

2) Extra Distance Searched Due to Conflict Resolution

To determine the extra distance searched for conflicts due to one conflict resolution for MVP, k_{cr}, consider the conflict situation and the corresponding MVP solution shown in Fig. 5. MVP uses the conflict geometry to compute an appropriate 'shortest-path' resolution vector that minimizes deviations from the nominal track. The conflict parameters shown in

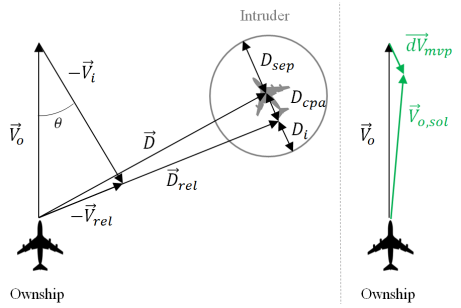

Fig. 5. Left: Parameters used to define a horizontal conflict. Right: Corresponding solution for the MVP CR algorithm. Adapted from [10]

Fig. 5 can be computed for a given conflict angle, θ, and distance to closest point of approach, D_{cpa}, as well as using the velocities of the ownship and intruder aircraft (taken to be equal in this study). For the situation shown, the relative velocity vector of can be calculated as:

$$\vec{V}_{rel} = \vec{V}_o - \vec{V}_i \tag{23}$$

Here, $\vec{V}_o$ and $\vec{V}_i$ are the (conflicting) velocity vectors of the ownship and intruder aircraft, receptively. These velocity vectors can be written as a function of the θ:

$$\vec{V}_o = \left[\bar{V}_{nr}, 0\right]^T \tag{24a}$$

$$\vec{V}_i = \left[\bar{V}_{nr}\cos(-\theta), \bar{V}_{nr}\sin(-\theta)\right]^T \tag{24b}$$

Subsequently, the distance between the ownship and the Closes Point of Approach (CPA), D_{rel}, and the corresponding position vector from the ownship, $\vec{D}_{rel}$, can be calculated as:

$$D_{rel} = t_l \cdot \left|\vec{V}_{rel}\right| + \sqrt{D_{sep}^2 - D_{cpa}^2} \tag{25a}$$

$$\vec{D}_{rel} = \frac{\vec{V}_{rel}}{|\vec{V}_{rel}|}\ D_{rel} \tag{25b}$$

The distance vector between the two aircraft, $\vec{D}$, can be computed using the property that $\vec{D}$, $\vec{D}_{rel}$ and $\vec{D}_{cpa}$ form a right angle triangle:

$$\vec{D} = \begin{bmatrix} D_{rel} & D_{cpa} \\ -D_{cpa} & D_{rel} \end{bmatrix} \cdot \frac{\vec{V}_{rel}}{|\vec{V}_{rel}|} \tag{26}$$

To minimize ownship path deviations, the MVP resolution velocity vector, $d\vec{V}_{mvp}$, is directed along $\vec{D}_{cpa}$, and is scaled such that the intrusion distance, D_i, is covered within the time to the closest point of approach, t_{cpa}:

$$d\vec{V}_{mvp} = \frac{D_i}{t_{cpa}} \cdot \frac{\vec{D}_{cpa}}{D_{cpa}} \tag{27}$$

Here, $\vec{D}_{cpa}$, t_{cpa} and D_i are defined as:

$$\vec{D}_{cpa} = \vec{D}_{rel} - \vec{D} \tag{28a}$$

$$t_{cpa} = \frac{D_{rel}}{|\vec{V}_{rel}|} \tag{28b}$$

$$D_i = D_{sep} - D_{cpa} \tag{28c}$$

Using $d\vec{V}_{mvp}$, the solution velocity vector with which the ownship should fly to resolve the conflict, $\vec{V}_{o,sol}$, can be computed:

$$\vec{V}_{o,sol} = \vec{V}_o + d\vec{V}_{mvp} \tag{29}$$

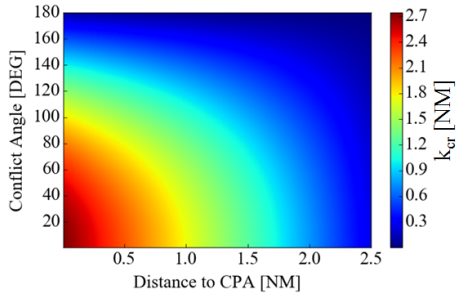

Fig. 6. Extra distance searched due to conflict resolution by MVP for $D_{sep} = 2.5$ nautical miles , $t_l = 5$ mins, and $V_{nr} = 500$ kts

Finally, the extra distance searched due to one CR maneuver with MVP, k_{cr}, can be calculated by comparing the distance traveled in the time needed to solve the conflict, t_{cpa}, for ownship velocities before and after resolution:

$$k_{cr}\left(\theta, D_{cpa}\right) = |\vec{V}_{o,sol}|t_{cpa} - |\vec{V}_o|t_{cpa} \tag{30}$$

This approach of calculating k_{cr} implies that aircraft fly trajectories parallel to their original flight tracks after the conflict is resolved, i.e., aircraft do no recover their pre-conflict flight paths. This is considered to be acceptable since most CR maneuvers using MVP result in very small path deviations.

Eq. 30 indicates that k_{cr} is dependent on θ and D_{cpa}. To understand this dependence, Eq. 30 is evaluated for the entire range of θ and D_{cpa}, for $D_{sep} = 2.5$ nautical miles (NM), $t_l = 5$ mins, and $V_{nr} = 500$ kts (the settings used for the 'Baseline' fast-time simulation, see section IV-C), see Fig. 6.

To calculate k_{cdr}, it is necessary to determine the *weighted-average* of the extra distance searched during one CR maneuver with MVP, $\bar{k}_{cr}$. This can be done by integrating Eq.30 over all θ and D_{cpa}, taking into account the distributions of θ and D_{cpa} for a decentralized direct-routing airspace concept:

$$\bar{k}_{cr} = \frac{\int_0^{D_{sep}} \int_0^{\pi} k_{cr}(\theta, D_{cpa}) W_\theta W_{D_{cpa}} \, d\theta \, dD_{cpa}}{\int_0^{D_{sep}} \int_0^{\pi} W_{D_{cpa}} W_\theta \, d\theta \, dD_{cpa}} \tag{31}$$

Here, $W_{D_{cpa}}$ and W_θ are the distributions of D_{cpa} and θ respectively. For a direct-routing airspace concept, there are no heading limitations on aircraft, and thus the headings of aircraft can be expected to follow a uniform distribution. Correspondingly, $W_{D_{cpa}}$ can be modeled as a uniform distribution, and W_θ should be modeled as a triangular distribution. Due to the highly nonlinear nature of the integrand of Eq.31, a numerical approach has been used to solve Eq.31 and compute $\bar{k}_{cr}$ in this work. Using a modern computer, this can be done within a few minutes for a reasonable discretization of θ and D_{cpa}.

It should be noted that for the values of V_{nr} and t_l used to compute Fig. 6, $k_{cd} = 41.67$ NM. Thus k_{cd} contributes more to k_{cdr} than k_{cr} when using state-based CD and MVP. This is logical as MVP, as stated earlier, uses shortest-path resolutions.

D. Modeling Capacity using the Domino Effect Parameter

Using the expressions developed for $C_{total_{wr}}$ and $C_{total_{nr}}$ in the previous paragraphs, a model for DEP can now be developed by substituting Eqs. 19 and 10 into Eq. 1:

$$DEP = \frac{\left(\bar{V}_{nr}\ T + \bar{L}_{nr}\right)(2T - t_l)}{\left(\bar{V}_{nr}\ T + \bar{L}_{nr}\right)(2T - t_l) - k_{cdr}\ \Upsilon} - 1 \tag{32}$$

To further analyze Eq. 32, λ and γ are defined to be equal to:

$$\lambda = \left(\bar{V}_{nr}\ T + \bar{L}_{nr}\right)(2T - t_l) \tag{33a}$$

$$\gamma = \frac{\rho_{ac} - \frac{1}{A}}{k_{cdr}\ \Upsilon} = \frac{1}{2\ k_{cdr} \cdot p_s \cdot D_{sep} \cdot \bar{V}_{nr} \cdot T^2} \tag{33b}$$

Substitution of Eq. 33 into Eq. 32 yields:

$$DEP = \frac{\rho_{ac} - \frac{1}{A}}{\lambda\gamma - \left(\rho_{ac} - \frac{1}{A}\right)} \tag{34}$$

Since $\rho_{ac} >> 1/A$ for most practical cases, Eq. 34 can be approximated as:

$$DEP \approx \frac{\rho_{ac}}{\lambda\gamma - \rho_{ac}} \tag{35}$$

In the above equation, the DEP, and therefore the number of conflict chain reactions, tends to infinity as the ρ_{ac} approaches $\lambda\ \gamma$. Therefore $\lambda\ \gamma$ is defined to be the maximum theoretical capacity of the airspace:

$$\rho_{max} = \lambda\gamma = \frac{\left(\bar{V}_{nr}\ T + \bar{L}_{nr}\right)(2T - t_l)}{2\ k_{cdr} \cdot p_s \cdot D_{sep} \cdot \bar{V}_{nr} \cdot T^2} \tag{36}$$

Here, k_{cdr} and p_s are modeled with Eqs. 21 and 4, respectively. Note that all terms in Eq. 36 have been fully defined in the derivation presented in this section. Also, on comparing Eqs. 3 and 36, the effect of the differences in the derivation process compared to that in [7] are evident.

IV. Fast-Time Simulation Design

Fast-time simulations of a 2D decentralized direct routing airspace concept were performed to validate the analytical capacity model derived in this paper. This section describes the design of this experiment.

A. Simulation Development

1) Simulation Platform

The BlueSky open-source ATM simulator, developed at TU Delft, was used as the simulation platform in this research. BlueSky has numerous features including the ability to simulate more than 5000 aircraft simultaneously with CD&R[1]. For more information on BlueSky, the reader is referred to [11].

2) Airborne Self-Separation Automation

As mentioned previously, state-based CD and the Modified Voltage Potential (MVP) CR algorithms are used in this study, see sections III-B and III-C for more details. It should be noted that CD was performed assuming perfect knowledge of aircraft states as a recent study concluded that ADS-B characteristics have little effect on the performance of the CD&R algorithms used here [12]. Since horizontal flight is considered, combined heading and speed conflict resolutions are used.

After a conflict was resolved, aircraft recovered their pre-conflict airspeed and heading, and flew trajectories parallel to their pre-conflict flight paths, i.e., they did not return to their pre-conflict trajectories. This was done to match the modeling of the k_{cr} term of the analytical capacity model, see section III-C2. Nonetheless, as MVP uses minimum-path deviation resolutions, the offset from the planned sector exit waypoint is not expected to be significant.

B. Traffic Scenarios

1) Testing Region and Flight Profiles

A large square en route sector of 500 x 500 NM was used as the physical environment for traffic simulations. A total of 396 entry/exit waypoints were defined on the edges of the sector, with a spacing of 5 NM (corner waypoints were intentionally removed). The trajectories of all traffic were required to cross

[1]BlueSky can be downloaded from https://github.com/ProfHoekstra/bluesky

TABLE I
SIMULATION PARAMETERS

Parameter	Value	Description
A	250,000 NM^2	Simulation area
$\bar{V}_{nr}$	550 kts	Speed when conflict free
$\bar{L}_{nr}$	435.5 NM	Average flight distance
T	1 hr	Analysis time duration
Δt_{sim}	0.05 s	Simulation time-step
Δt_{cdr}	1.00 s	CD&R time-step

the square sector with direct routes i.e., for a particular aircraft, the entry and exit waypoint could not be located on the same side of the sector. When an aircraft exited the sector, it was deleted from the simulation. Additionally, all aircraft flew at the same speed when conflict-free, see Table I.

2) Scenario Generation

A scenario generator was created to produce traffic scenarios with a desired and constant traffic density, and with a uniform heading distribution. Constant density scenarios were required so that total the number of conflicts logged during a simulation run could be attributed to a particular density, and a uniform heading distribution was required to ensure that there were no preferred directions in a scenario, as would be the case for decentralized direct-routing airspace.

Since aircraft were deleted from the simulation as they exited the sector, to realize constant density scenarios, aircraft were introduced into the simulation at rate, ω_{ac}, equal to:

$$\omega_{ac} = \frac{\rho_{ac} A \bar{V}_{nr}}{\bar{L}_{nr}} \tag{37}$$

Here, ρ_{ac} is the desired traffic density, A is the airspace area used for simulation, $\bar{V}_{nr}$ is average aircraft speed and $\bar{L}_{nr}$ is average flight distance through the sector. These and other constant simulation parameters are listed in Table I. Using this approach, ten traffic demand scenarios of increasing density were defined, see Table II.

To create scenarios with uniform heading distributions, it was necessary to ensure that there were no biases in selecting entry and exit waypoints for aircraft. This was achieved in three steps. In the first step, the number of available exit points per entry point was kept the same for all waypoints. Given the constraint that all aircraft routes had to cross the square sector, corner waypoints were removed. In this way, 297 exit points met this constraint for all waypoints. In the second step, the entry point for each aircraft was selected using a uniformly distributed random variable, and a particular entry point could only be selected multiple times if all other entry points had been selected once before. In the final step, all exit points meeting the aforementioned routing constraint for a particular entry point were assigned an equal probability of being selected. Fig. 7 illustrates the heading distribution of a representative simulation scenario. Kolmogorov-Smirnov tests

TABLE II
TRAFFIC DEMAND SCENARIOS

#	Density [ac/10,000 NM^2]	Number of Instantaneous AC
1	1.00	25.00
2	1.51	37.67
3	2.27	56.75
4	3.42	85.50
5	5.15	128.82
6	7.76	194.08
7	11.70	292.40
8	17.62	440.54
9	26.55	663.73
10	40.00	1000.00

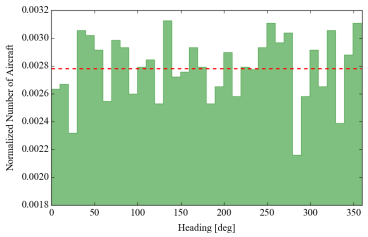

Fig. 7. Heading distribution of representative scenario. Scenarios were designed to have uniform heading distributions.

TABLE III
EXPERIMENT CONDITIONS

Condition Name	Separation Minimum D_{sep} [NM]	Look-Ahead t_l [mins]
Baseline	2.5	5.0
Half Look-Ahead	2.5	2.5
Double Separation	5.0	5.0

confirmed that the above approach produced uniform heading distributions; D = 0.0076, p>0.05 for the distribution in Fig. 7.

C. Independent Variables

Two independent variables were defined for the experiment. The first independent variable was traffic demand density, for which ten scenarios have been defined, see Table II. The second independent variable was concerned with the settings used for CD&R, namely look-ahead time and horizontal separation minimum. Using different combinations of these two parameters, three experiment conditions have been defined, see Table III.

For each demand density, ten repetitions were performed using different traffic realizations. Additionally, each scenario was simulated with and without CR to compute the DEP. This resulted in a total of 600 simulation runs (ten demand scenarios $\times$ three CD&R conditions $\times$ ten repetitions $\times$ two CR settings).

D. Dependent Variables

To validate different components of the analytical capacity model derived in section III, model predictions for the following six dependent variables are compared to that of the previous semi-empirical capacity measurement method:

1) Global instantaneous conflict rate without conflict resolution, $C_{ss_{nr}}$, Eq. 5
2) Total number of conflicts without conflict resolution, $C_{total_{nr}}$, Eq. 10
3) Total number of aircraft with and without conflict resolution, $N_{total_{wr}}$ and $N_{total_{nr}}$, Eq. 13
4) Local conflict rate with and without conflict resolution, $r_{c_{wr}}$ and $r_{c_{nr}}$, Eq. 14
5) Extra distance searched with per conflict resolution maneuver, k_{cdr}, Eq. 21
6) Airspace capacity, ρ_{max}, Eq. 36

E. Simulation Procedure and Data Logging

To minimize unsystematic variation in the results, standardized simulation conditions were used. For a particular repetition of a traffic demand scenario, the creation times of aircraft and entry/exit waypoint combinations were kept constant across all three experiment conditions. Additionally, scenarios had a duration of 2.5 hours, consisting of a 1.5hr traffic volume buildup period and a 1hr logging period.

Two types of conflict logging were used. Periodic logging was used to record the number of active conflicts and aircraft in the air every 15 seconds, and was used to compute the global instantaneous conflict rate. All other dependent variables were

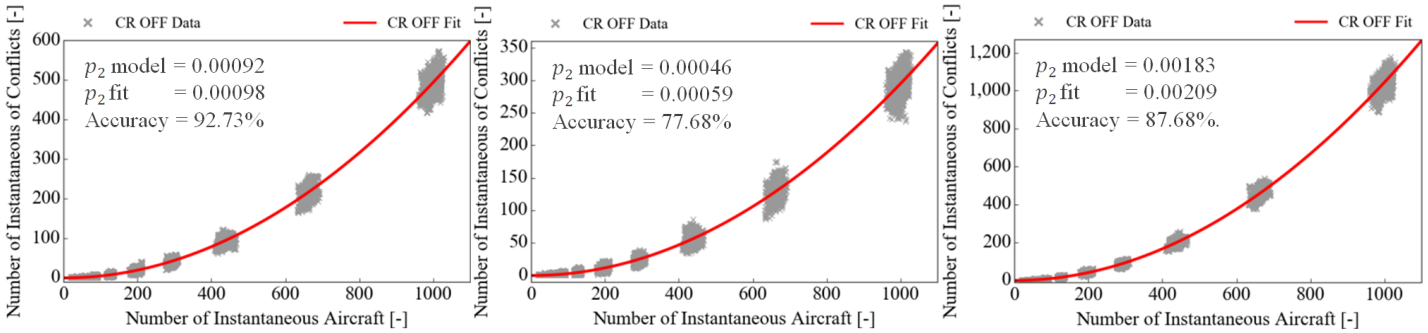

(a) Baseline Experiment (b) Half Look-Ahead Experiment (c) Double Separation Experiment

Fig. 8. Global instantaneous conflict rate without CR. Experiment conditions are described in Table III. Scatter: simulation data; Curve: LSF to Eq. 5.

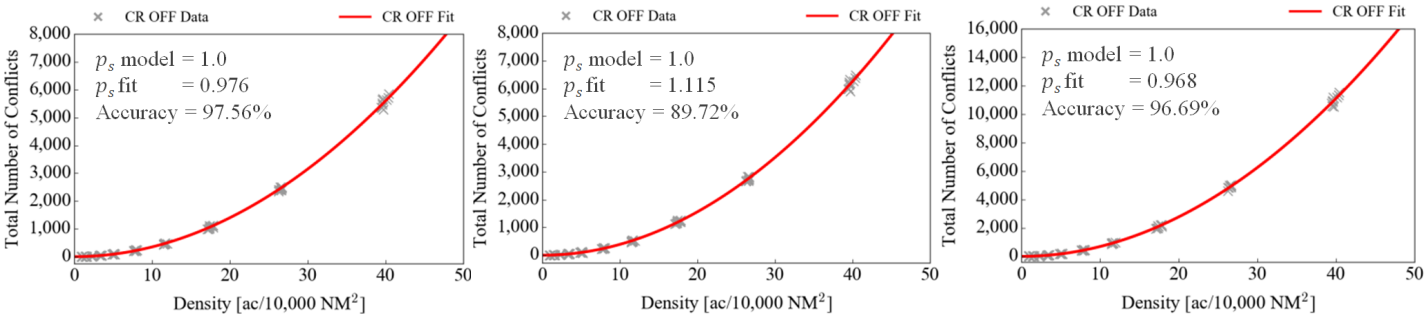

(a) Baseline Experiment (b) Half Look-Ahead Experiment (c) Double Separation Experiment

Fig. 9. Total number of conflicts without CR. Experiment conditions are described in Table III. Scatter: simulation data; Curve: LSF to Eq. 10.

computed using conflict data from event-driven logging, which kept track of the properties of conflicts as soon as they occurred.

It should be noted that conflicts with CPAs outside the simulation area were not logged or resolved because the traffic density was zero outside the simulation area. On a similar note, pop-up conflicts at the start of an aircraft's flight, with a look-ahead distance less than $V_{nr}t_l$, were also not logged or resolved, since these conflicts occurred due to the finite simulation area used. All other conflicts, including multiple conflicts between the same aircraft pair, were used logged, resolved and used in the analysis.

V. Results and Discussion

Using data from the fast-time simulations, the absolute accuracy of the analytical capacity model, Ψ_{model}, is assessed by comparing it to the previous semi-empirical method using the following simple expression:

$$\Psi_{model} = 100\% - \frac{|\varepsilon_{model} - \varepsilon_{fit}|}{\varepsilon_{fit}} \tag{38}$$

Here, ε_{model} is the model prediction, and ε_{fit} is the Least-Square Fit (LSF) of the semi-empirical method to the simulation data, for a particular airspace state. Additionally, all figures display the LSF curve of the appropriate model to the simulation data (scatter points). Thus, the shape of the LSF curve relative to the simulation data is an indication of overall 'soundness' of the modeling approach used by both the analytical and semi-empirical modeling methods, while the absolute accuracy of the analytical model can be evaluated using the above equation.

A. Global Instantaneous Conflict Rate Without Conflict Resolution

The results for the global instantaneous conflict rate without CR, $C_{ss_{nr}}$, are displayed in Fig. 8. The model for $C_{ss_{nr}}$ is given by Eq. 5. The accuracy of the model is determined by comparing the LSF value of the p_2 term in Eq. 5, which is the instantaneous conflict probability between any two aircraft, to the p_2 value computed using the model given by Eq. 6.

From the shape of the curves in Fig. 8, it can be concluded that the general structure of Eq. 5 well represents $C_{ss_{nr}}$ for all three experiment conditions, and that changes to the look-ahead time and the separation minimum have proportional changes to the global conflict rate, as suggested by the analytical model of p_2. Moreover, the absolute accuracy of the analytical model for p_2 is found to be quite high for the 'Baseline' and 'Double Separation' experiments. On the other hand, it is less accurate for the 'Half Look-Ahead' experiment. This suggests that the 'conflict search area' for state-based CD in the p_2 model is sensitive to changes to the look-ahead time and may not be well approximated by a rectangular shape, see Fig 2. An explanation for this is given in section V-G.

B. Total Number of Conflicts Without Conflict Resolution

Fig. 9 shows the results for the total number of conflicts without CR, $C_{total_{nr}}$. The corresponding model for $C_{total_{nr}}$ is given by Eq. 10. Model accuracy is evaluated by comparing the LSF value of the p_s term in Eq. 10, which is the effect of traffic structure on instantaneous conflict probability, to the p_s value computed analytically using its model in Eq. 4.

The curves in Fig. 9 well represent the relationship between $C_{total_{nr}}$ and traffic density, indicating that the overall structure of Eq. 10 is valid. Once again, model accuracy is shown to be quite high for the 'Baseline' and 'Double Separation' experiments, and is the lowest for the 'Half Look-Ahead' experiment. Nevertheless, in contrast to the global conflict rate without CR, accuracy is greater than 85% for all cases. This is explained by considering the expression for $C_{total_{nr}}$ in Eq. 10. Here it can be seen that a change in the look-ahead time only affects $C_{total_{nr}}$ if the difference between the total analysis time (during which conflicts are counted) and the look-ahead time is small. This is not the case for the 'Half Look-Ahead'

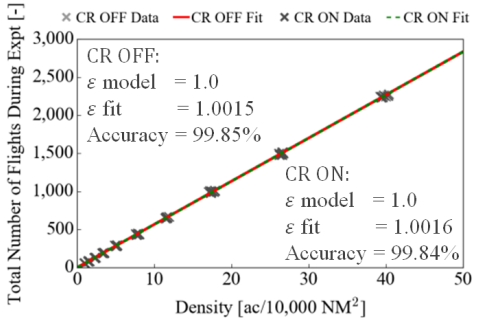

Fig. 10. Total number of aircraft with and without CR for the 'Baseline' experiment. Scatter: simulation data; Curve: LSF to Eq. 13.

TABLE IV
ACCURACY OF THE LOCAL CONFLICT RATE MODEL

		Baseline	Half Look-Ahead	Double Separation
CR OFF	ε_{model}	1.0	1.0	1.0
	ε_{fit}	0.973	1.113	0.967
	Accuracy	97.24%	89.82	96.59
CR ON	ε_{model}	1.0	1.0	1.0
	ε_{fit}	1.216	1.250	1.303
	Accuracy	82.27%	79.99%	76.75%

experiment, for which the analysis time is 24 times larger than the look-ahead time. This also explains why the 'Half Look-Ahead' experiment shows no significant differences to the 'Baseline' experiment in terms of $C_{total_{nr}}$, see Fig. 9.

C. Total Number of Aircraft with and without Conflict Resolution

Results for the total number of aircraft simulated during the 1hr logging/analysis period are displayed in Fig. 10 for the 'Baseline' simulation condition. Results for the other two conditions are similar, but are not shown because the corresponding model is not dependent on CD&R parameters, see Eq. 13. The figure shows that Eq. 13 is very accurate in predicting the total number of aircraft for the cases with and without CR. Therefore, the first assumption used in the derivation of $C_{total_{wr}}$, which is the total number of conflicts *with* CR, that $N_{total_{wr}} \approx N_{total_{nr}}$, is valid for all considered densities and experiment conditions.

D. Local Conflict Rate With and Without Conflict Resolution

The results for the local conflict rate per unit distance with and without CR, $r_{c_{wr}}$ and $r_{c_{nr}}$, are pictured in Fig. 11. The corresponding model is given by Eq. 14, and the model accuracy results are listed separately for the CR OFF and CR ON cases in Table IV.

The results show that the analytical model is very accurate in predicting the local conflict rate without CR (CR OFF), $r_{c_{nr}}$, for all three experiment conditions. However Table IV shows this is not true for the case with CR (CR ON), for which the lowest accuracy is found for the 'Double Separation' experiment.

An important assumption used in the derivation by *both the analytical and semi-empirical models*, is that $r_{c_{nr}} \approx r_{c_{wr}}$. However, Fig. 11 shows that this assumption is only true at relatively 'low' densities. For instance, if the model for $r_{c_{wr}}$ is fitted to the simulation data for densities up to 11.7 aircraft per 10,000 NM^2, i.e., for densities on the left side of the blue dashed line in Fig. 11c, then the accuracy for the 'Double Separation' experiment would equal 89.66%. Therefore, the low overall accuracy for $r_{c_{wr}}$ can be attributed to the breakdown of the aforementioned assumption at high densities. An explanation for this is given in section V-G.

E. Extra Distance Searched Per Conflict Resolution Maneuver

Unlike the other dependent variables, no explicit expression for k_{cdr} in terms of CD&R characteristics was developed in the previous semi-empirical capacity measurement method. In fact, the analytical modeling of k_{cdr} is a additional step added to derivation procedure of the semi-empirical method. Therefore, to determine the accuracy of the analytical k_{cdr} model, the average k_{cdr} logged for all the conflicts during the simulations is compared to model predictions, see Table V. Note that the analytical model for k_{cdr} is given by Eq. 21, which is in turn defined in terms of k_{cd} using Eq. 22 for state-based CD, and $\bar{k}_{cr}$ using Eq. 31 for the MVP CR algorithm.

Table V indicates that the predictions of the analytical k_{cdr} model are very close to the average values logged during the simulations for all three experiment conditions. Since k_{cdr} is inversely related to airspace stability, the derivation procedure described in section III-C can thus be used to understand the effect of changes to CD&R parameters on conflict chain reactions.

It is interesting to note from Table V that a change in look-ahead time, t_l, has a much larger effect on k_{cdr} than an equivalent change to the separation minimum, D_{sep}. This is because the MVP CR algorithm used in this work resolved conflicts with minimum path deviations, resulting in low k_{cr} for practical values of D_{sep} and t_l. On the other hand, t_l has a direct and proportional influence on CD, and thus also on k_{cd}, see Eq. 22. Thus, for the CD and CR algorithms used in this study, CD has a greater influence on stability than CR.

F. Airspace Capacity

The final dependent variable to be considered is airspace capacity. Airspace capacity, ρ_{max}, is determined for the semi-empirical capacity measurement method by determining the density at which the Domino Effect Parameter (DEP) model of Eq. 34 tends to infinity. For the analytical model, ρ_{max} can be computed using Eq. 36. Fig. 12 displays the DEP results and the accuracy of the analytical capacity model for all three experiment conditions.

Figs 12a and 12b indicate that the analytical model estimates ρ_{max} with high accuracy for the 'Baseline' and 'Look-Ahead' experiments. However the capacity accuracy for the 'Double-Separation' experiment is very low, with the model underestimating ρ_{max} by almost 53%. As for the local conflict rate with CR, the low accuracy for the 'Double Separation' experiment is due to the breakdown of the $r_{c_{nr}} \approx r_{c_{wr}}$ assumption at higher traffic densities. For instance, if a model fit is performed for simulation densities less than 11.7 aircraft per 10,000 NM^2, i.e., for densities on the left side of the blue dashed line in Fig. 12c, where the local conflict rate assumption holds, then the accuracy for 'Double Separation' is 94.61%.

G. Results Analysis and Discussion

From the above results, the following effects were observed:

Model accuracy without CR is affected by look-ahead time
The model accuracy *without* Conflict Resolution (CR) was reduced when the look-ahead time was changed from its baseline value. This could be caused by differences in the definitions used for Conflict Detection (CD) by the model and in the simulation. In the model, a conflict is defined to occur at time t_{cpa} when the minimum distance point between two conflicting aircraft falls within a rectangular 'conflict search area', see Fig. 2. However, in the simulation, the first moment

TABLE V
ACCURACY OF THE EXTRA DISTANCE SEARCHED MODEL

	Baseline	Half Look-Ahead	Double Separation
k_{cdr} **Model [NM]**	46.68	23.78	47.55
k_{cdr} **Sim Average [NM]**	46.50	23.63	47.20
Accuracy	99.61%	99.41%	99.24%

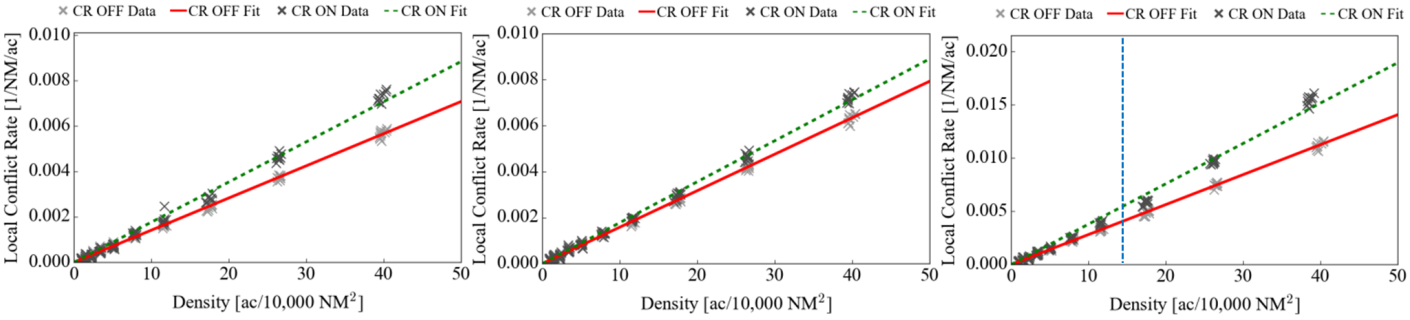

(a) Baseline Experiment (b) Half Look-Ahead Experiment (c) Double Separation Experiment

Fig. 11. Local conflict rate per unit distance and per flight, with and without CR. Experiment conditions are described in Table III. Model accuracy results are listed in Table IV. Scatter: simulation data; Curve: LSF to Eq. 14.

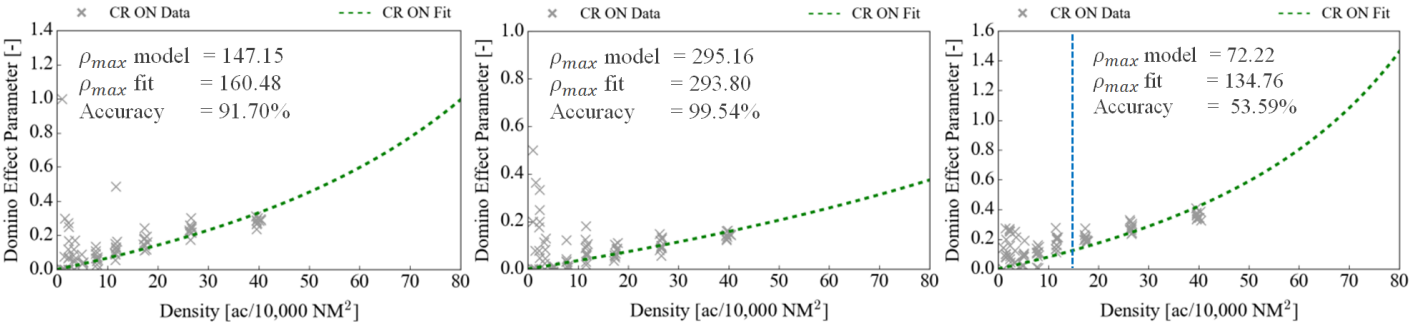

(a) Baseline Experiment (b) Half Look-Ahead Experiment (c) Double Separation Experiment

Fig. 12. Domino Effect Parameter (DEP) and capacity estimate. Experiment conditions are described in Table III. Scatter: simulation data; curve: LSF to Eq. 34.

of conflict detection occurs at time $t_{in_{conf}}$ when the separation requirements are about to be violated. Conflicts are detected in the simulation earlier than for the approach used by the model, see Fig. 13. As the difference between t_{cpa} and $t_{in_{conf}}$ increases for shallow conflict angles, it is hypothesized that a *trapezoidal* conflict search area needs to be used to improve model accuracy. This hypothesis will be investigated in future research.

The local conflict rate is dependent on conflict resolution

One of the main assumptions used by the current analytical model, and by the previous semi-empirical method, is that the local conflict rate per unit distance with and without CR are equal. The current results, however, indicate that this assumption is not entirely valid, and CR increased the local conflict rate at higher densities. This in turn reduced the accuracy of the capacity model for the 'Double Separation' experiment.

An explanation for the breakdown of this assumption at high densities can be found by comparing the traffic density contours for the three experiment conditions, see Fig. 14. This figure shows that CR had no significant effect on the density distribution for the 'Baseline' and 'Half Look-Ahead' experiments. On the other hand, for the Double Separation' experiment, conflict resolution led to fewer density hot-spots. This is because doubling the separation requirement implicitly quadruples the traffic density when considering amount of airspace occupied by each aircraft, for the same number of instantaneous aircraft as for the other two experiments. This implicit increase in density leads to an increase in conflicts, and conflict chain reactions. For voltage-potential based CR algorithms, the consequent increase in the number of resolution maneuvers at high densities leads to a 'spreading-out' of traffic. Near the edges of the simulation area, aircraft are therefore 'bounced' out of the experiment, at which point they are deleted. The resulting pre-mature deletion of aircraft reduces

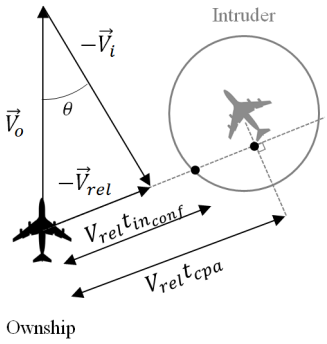

Fig. 13. Difference between t_{cpa}, the time to Close Point of Approach (CPA), and $t_{in_{conf}}$, the first moment of a predicted loss of separation

the rate of growth of the *measured* DEP, which in turn leads to a higher capacity estimate when fitting the DEP model to the simulation data compared the analytical model.

Thus, the local conflict rates with and without CR are not equal at high densities due to the strong traffic 'dispersion' effect caused by conflict chain reactions. To improve the accuracy of the model at high densities/separation requirements, this effect needs to be taken into account. Furthermore, simulations used to validate such models should be designed such that aircraft are not prematurely deleted when they are 'bounced' out of the simulation sector as a result of CR maneuvers. Instead, the distance-to-destination can be used to avoid premature deletion of aircraft.

Model can be used to understand the factors influencing capacity

Despite the limitations discussed above, the current form of the analytical model can be used to determine a first order capacity estimate when reduced separation requirements can be used, as would be the case for future urban air transportation systems.

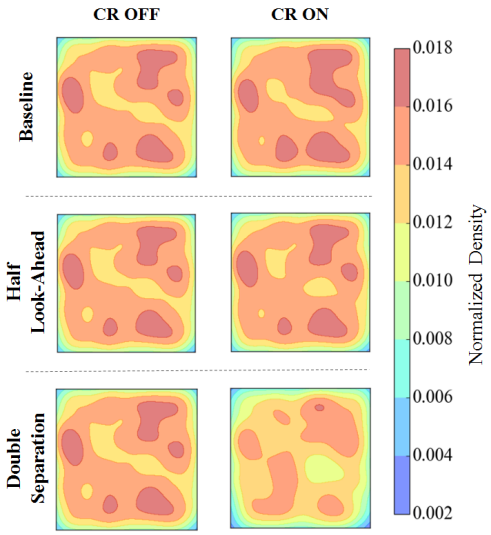

Fig. 14. Traffic density contour for the three experiment conditions at the same time instant of a representative repetition of the highest traffic demand, with and without CR

Furthermore, the model can be used to understand the factors that affect airspace capacity for decentralization. For instance, the model predicted, and the simulation proved, that 'state-based' CD had a greater effect on stability, and consequently on airspace capacity, than the MVP CR algorithm. Since state-based CD is influenced by the look-ahead time, an optimization of look-ahead time with traffic density could be performed to maximize capacity. In this way, the model can be used to select a subset of the available airspace design-space for further investigation using fast-time simulations.

Theoretical vs. practical capacity

While the models addressed here focus on the theoretical capacity limit of direct-routing decentralized airspace, in practice, society will not accept an asymptotic limit of airspace stability as an indication of the achievable capacity. Moreover, airline economics, which is primarily focused on improving efficiency, and stochastic elements, such as weather, affect the practical airspace capacity. Nevertheless, determining the theoretical capacity limit is useful as a metric for comparing different forms of decentralization and/or CD&R algorithms.

VI. Conclusions and Recommendations

In this study, an analytical capacity model was derived for a decentralized direct-routing airspace concept for motion in the horizontal plane. This model is an extension of a semi-empirical method reported in literature. Fast-time simulation experiments were conducted to validate the derived model and its components. The following conclusions can be drawn:

- The theoretical capacity limit of decentralized airspace can be defined as the density at which the Domino Effect Parameter (DEP) , a measure of airspace stability, approaches infinity. At this density, all aircraft in the airspace exist in a state of conflict due to conflict chain reactions.
- Simulation results showed that the model accurately predicts the extra distance searched for conflicts due to conflict resolution maneuvers. Therefore, the model can be used to understand the effect of Conflict Detection and Resolution (CD&R) parameters on conflict chain reactions and airspace stability.
- For the conflict detection and conflict resolution algorithms considered in this study, conflict detection had greater impact on airspace stability.
- The accuracy of derived analytical capacity model is sufficient to gain a first order estimate of capacity for decentralization, and provides insights on the effect of different airspace and CD&R parameters on capacity.
- The scope and accuracy of the model can be increased by taking into account the effect of conflict chain reactions on the local, or per aircraft, conflict rate. This will be considered in future research, as will extending the model for three-dimensional airspace.

References

[1] J. M. Hoekstra, R. N. H. W. van Gent, and R. C. J. Ruigrok, "Designing for safety: the free flight air traffic management concept," *Reliability Engineering & System Safety*, vol. 75, no. 2, pp. 215–232, Feb. 2002.

[2] J. M. Hoekstra, R. C. J. Ruigrok, and R. N. H. W. van Gent, "Free Flight in a Crowded Airspace?" in *Proceedings of the 3rd USA/Europe Air Traffic Management R&D Seminar*, Naples, Jun. 2000.

[3] M. Ballin, J. Hoekstra, D. Wing, and G. Lohr, "NASA Langley and NLR Research of Distributed Air/Ground Traffic Management," in *AIAA Aircraft Technology, Integration, and Operations (ATIO) Conference, AIAA-2002-5826*. American Institute of Aeronautics and Astronautics, 2002.

[4] J. K. Kuchar and L. C. Yang, "A Review of Conflict Detection and Resolution Modeling Methods," *IEEE Transactions on Intelligent Transportation Systems*, vol. 1, pp. 179–189, 2000.

[5] J. Krozel, M. Peters, and K. Bilimoria, "A decentralized control strategy for distributed air/ground traffic separation," in *AIAA Guidance, Navigation, and Control Conference and Exhibit*. American Institute of Aeronautics and Astronautics, 2000.

[6] K. Bilimoria, K. Sheth, H. Lee, and S. Grabbe, "Performance evaluation of airborne separation assurance for free flight," in *AIAA Guidance, Navigation and Control Conference, AIAA-2000-4269*, 2000.

[7] M. R. Jardin, "Analytical Relationships Between Conflict Counts and Air-Traffic Density," *Journal of Guidance, Control, and Dynamics*, vol. 28, no. 6, pp. 1150–1156, 2005. [Online]. Available: http://dx.doi.org/10.2514/1.12758

[8] E. Sunil, J. Ellerbroek, J. Hoekstra, A. Vidosavljevic, M. Arntzen, F. Bussink, and D. Nieuwenhuisen, "Analysis of Airspace Structure and Capacity for Decentralized Separation Using Fast-Time Simulations," *Journal of Guidance, Control, and Dynamics*, vol. 40, no. 1, pp. 38–51, 2017. [Online]. Available: http://dx.doi.org/10.2514/1.G000528

[9] Hoekstra, J., Maas, J., Tra, M., and Sunil, E., "How Do Layered Airspace Design Parameters Affect Airspace Capacity and Safety?" in *Proceedings of the 7th International Conference on Research in Air Transportation*, Jun. 2016.

[10] J. Ellerbroek, "Airborne Conflict Resolution in Three Dimensions," Ph.D. dissertation, Delft University of Technology, Faculty of Aerospace Engineering, Sep. 2013. [Online]. Available: http://resolver.tudelft.nl/uuid:96c65674-06d4-410c-87c2-b981af95211e

[11] J. Hoekstra and J. Ellerbroek, "BlueSky ATC Simulator Project: an Open Data and Open Source Approach," in *Proceedings of the 7th International Conference on Research in Air Transportation*, Jun. 2016.

[12] T. Langejan, E. Sunil, J. Ellerbroek, and J. Hoekstra, "Effect of ADS-B Characteristics on Airborne Conflict Detection and Resolution," in *Proccedings of the 6th Sesar Innovation Days*, 2016.

Author Biographies

Emmanuel Sunil received the MSc degree in Aerospace Engineering (cum laude) from TU Delft in 2014, for his work on a haptic interface for unmanned aircraft collision avoidance. He is currently a PhD candidate at the faculty of Aerospace Engineering, TU Delft. His work focuses on airspace design and capacity modeling.

Joost Ellerbroek received the M.Sc. (2007) and Ph.D. (2013) degrees in aerospace engineering from the Delft University of Technology, The Netherlands, with the Control and Simulation section, where he is currently working as an Assistant Professor. His research interests lie in the field of Air Traffic Management, and include topics such as the analysis of airspace complexity and capacity, data science in ATM, the design and analysis of conflict detection and resolution algorithms, and human-automation interaction.

Jacco Hoekstra obtained his MSc, PhD and private pilot license from TU Delft. He has worked at the Dutch National Aerospace Laboratory (NLR) for 16 years, and has co-operated with NASA, the FAA and many European organizations. He founded the Association for Scientific Development of ATM, was the founding director of AT-One and was the head of NLR's Air Transport Division. After serving two terms as dean of the Aerospace Engineering faculty of TU Delft, he is now a full professor at this faculty, and holds the chair in CNS/ATM. His research topics include 4D trajectory based ATM, airborne separation assurance and controller-pilot data link communication. Next to research, he teaches courses on CNS/ATM, programming in Python and aeronautics.

Jerom Maas received the MSc degree in Aerospace Engineering from TU Delft in 2015, for his work on augmenting swarming logic to a voltage potential-based airborne conflict resolution algorithm. He is currently a PhD candidate at the faculty of Aerospace Engineering, TU Delft, where he is developing an obstacle detection radar system to aid general aviation pilots with VFR tasks.